Vapor grown carbon nanofiber based cotton fabrics with negative thermoelectric power

A. J. Paleo, E. M. F. Vieira, K. Wan, O. Bondarchuk, M. F. Cerqueira, E. Bilotti, M. Melle-Franco & A. M. Rocha

ONLINE FIRST

Springer

Springer

ORIGINAL RESEARCH

Vapor grown carbon nanofiber based cotton fabrics with negative thermoelectric power

A. J. Paleo (ORCID) · **E. M. F. Vieira · K. Wan · O. Bondarchuk · M. F. Cerqueira ·
E. Bilotti · M. Melle-Franco · A. M. Rocha**

Abstract Vapor grown carbon nanofiber (CNF) based ink dispersions were used to dip-coat woven cotton fabrics with different constructional parameters, and their thermoelectric (TE) properties studied at room temperature. Unlike the positive thermoelectric power (TEP) observed in TE textile fabrics produced with similar carbon-based nanostructures, the CNF-based cotton fabrics showed negative TEP, caused by the compensated semimetal character of the CNFs and the highly graphitic nature of their outer layers, which hinders the p-type doping with oxygen groups onto them. A dependence of the electrical conductivity (σ) and TEP as a function of the woven cotton fabric was also observed. The cotton fabric with the largest linear density (tex) showed the best performance with negative TEP values around $-8\ \mu V\ K^{-1}$, a power factor of 1.65×10^{-3} $\mu W\ m^{-1}\ K^{-2}$, and a figure of merit of 1.14×10^{-6}. Moreover, the possibility of a slight e^- charge transfer or n-doping from the cellulose onto the most external CNF graphitic shells was also analysed by computer modelling. This study presents n-type carbon-based TE textile fabrics produced easily and without any functionalization processes to prevent the inherent doping with oxygen, which causes the typical p-type character found in most carbon-based TE materials.

A. J. Paleo (✉) · A. M. Rocha
2C2T-Centre for Textile Science and Technology, University of Minho, Campus de Azurém, 4800-058 Guimarães, Portugal
e-mail: ajpaleovieito@2c2t.uminho.pt

E. M. F. Vieira
CMEMS-UMinho-Center for MicroElectromechanical Systems, University of Minho, Campus de Azurém, 4800-058 Guimarães, Portugal

K. Wan · E. Bilotti
SEMS-School of Engineering and Material Sciences, Queen Mary University of London, Mile End Road, London, UK

O. Bondarchuk · M. F. Cerqueira
INL-International Iberian Nanotechnology Laboratory, Av. Mestre. Jose Veiga, Braga, Portugal

M. F. Cerqueira
CFUM – Center of Physics of the University of Minho, Campus de Gualtar, 4710-057 Braga, Portugal

M. Melle-Franco
CICECO – Aveiro Institute of Materials, Department of Chemistry, University of Aveiro, 3810-193 Aveiro, Portugal
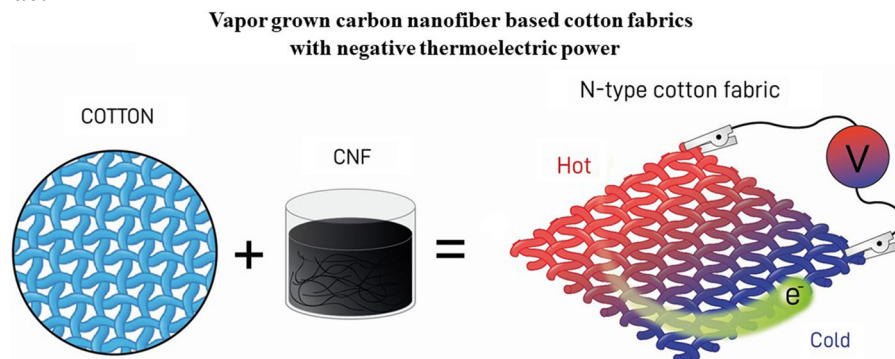
Springer

Graphic abstract

Vapor grown carbon nanofiber based cotton fabrics with negative thermoelectric power

Introduction

Wearable thermoelectric (TE) devices that transform the temperature gradient between the human body and surrounding environment into an electrical voltage, determined by the Seebeck coefficient (α) or thermo-electric power (TEP), and calculated as $\alpha = \frac{\Delta V}{\Delta T}$ (Beretta et al. 2019), have emerged as excellent candidates to power portable electronics (Kim et al. 2018; Ryan et al. 2017). In order to fabricate thermoelectric generators (TEG), both p-type TE materials with positive α (hole-transporting) and n-type TE materials with negative α (electron-transport-ing), are required (Blackburn et al. 2018). The efficiency of a TE material is rated by its dimension-less figure of merit $zT = \frac{\alpha^2 \sigma}{k} T$, where $\alpha^2 \sigma$ is known as the power factor (PF), T is the absolute temperature, and k is the thermal conductivity (Rowe 1995). At present, materials such as bismuth telluride (Bi_2Te_3), with zT around 1, are the most used inorganic semiconductors in the production of TEG (Francioso et al. 2013; Snyder and Toberer 2008; Yee et al. 2013). However, the combination of their high k, harmful-ness, brittleness and expansive costs, have raised the interest in finding substitute TE materials (Li et al. 2019; McGrail et al. 2015; Veluswamy et al. 2019). It is in this scenario that the exploration of carbon nanotubes (CNTs) as new TE materials has flourished appreciably thanks to their high theoretical TEP and the option of tuning their α by diverse doping approaches (Kang et al. 2005). Nevertheless, one critical handicap of CNTs is their high k around 2000 W/mK (Yu et al. 2005), which diminishes greatly their zT. It is for this reasoning that their integration into textile fabrics is contemplated as an attractive choice for the production of wearable TE devices by virtue of the high electrical conductivity (σ) and α brought by CNTs, and the low k and flexibility of the textile fabric (Cataldi et al. 2019; Lan et al. 2019; Li et al. 2016; Wang et al. 2019), and among natural fibers, cotton-based textile fabrics are drawing strong attention for the realization of wear-able TE devices (Cataldi et al. 2019; Karttunen et al. 2017; Wu and Hu 2016). On the other hand, most of studies on CNT-based textiles are p-type TE materials due to the extreme oxygen sensitivity of CNTs (Zettl 2000). For instance, positive TEP of around 12 $\mu V\ K^{-1}$ were reported for as-treated polyesters immersed in a solution of single wall carbon nan-otubes (SWCNTs) and polyaniline (PANI) (Li et al. 2016). A positive Seebeck coefficient of 10 $\mu V\ K^{-1}$ was found for composites films made of waterborne polyurethane (WPU), multiwall carbon nanotubes (MWCNTs) and poly(3,4-ethylenedioxythiophene)-poly(styrenesulfonate) (PEDOT:PSS), a composition which was used after for producing inks to dip-coat polyester and cotton yarns (Wu and Hu 2016). Higher positive values of around 40 μVK^{-1} were achieved for CNT-based yarns made by wet-spinning of SWCNTs and polyethylene glycol (PEG) (Ito et al. 2017). On the contrary, reports of n-type CNT-based TE textiles are more scarce due to the mentioned oxygen doping of CNTs. Among the few studies, we can highlight one work that describes n-type CNT-based yarns of

SWCNT/PEG doped with 1-butyl-3-methylimida-zolium hexafluorophosphate ([BMIM]PF6), where negative TEP above -40 μV K^{-1} (absolute value) were achieved (Ito et al. 2017). Another study shows n-type yarns of -14 μV K^{-1} obtained by coating commercial poly(ethylene terephthalate) (PET) sewing threads with MWCNTs and poly(N-vinylpyrrolidone) (PVP) (Ryan et al. 2018). Therefore, the development of air-stable n-type TE textiles based on CNTs remains a challenge. On the other hand, in spite of the enormous interest in the use of CNTs as novel TE materials already mentioned, very limited efforts were approached on the TE study of a different carbon nanostructure known as carbon nanofibers (CNFs). CNFs normally present larger diameters than CNTs and diverse orientation of the graphitized shells with respect to their hollow tubular axis. The most common routes of CNFs synthesis are chemical vapor deposition (CVD) (Tibbetts et al. 2007), electrospinning (Miao et al. 2010), and laser ablation (Minus and Kumar 2005). This general lack of research of TE materials based on CNFs results very surprising since it is known for some time that heat-treated benzene-derived carbon fibers prepared by thermal decomposition (Endo et al. 1977), heat-treated graphite fibers grown by pyrolysis of natural gas (Heremans and Beetz Jr 1985), and heat treated methane-derived vapor grown carbon fibers (VGCF) produced by CVD (Stokes et al. 1996), showed air-stable negative TEP at room temperature. Accordingly, the principal objective of this study is to fill the current absence of works focused on the TE properties of CNF-based textiles, and then to extend our recently published TE results of CNFs and polypropylene (PP) composites produced by melt mixing (Paleo et al. 2019). In that study, we demonstrated that it is possible to generate n-type polymer composites with low contents of CNFs and with TEP up to -8.5 μV/K without any functionalization/doping of CNFs or other further additives during processing. In this study, three different types of common cotton woven fabrics were dip-coated with the same CNF-based ink dispersion and their thermoelectric properties (i.e. TEP, PF and zT) characterized at room temperature. In accordance with our previous results on the n-type TE behavior of melt-extruded PP/CNF composites, we demonstrate herein that the dip-coated CNF-based cotton fabrics also show n-type TE behavior. To the best of our knowledge, this is the first study that reports n-type carbon-based TE textile fabrics without the utilization of any functionalization process and additives to avoid the inherent doping with oxygen, which causes the typical hole-transporting character found in most carbon-based TE materials.

Materials and methods

Materials

100% cotton woven fabric with three different warp x weft yarns linear densities (tex) named as CWF1, CWF2 and CWF3 as provided by the manufacturer were used as support materials. Specific constructional parameters and physical properties of the fabrics are listed in Table 1. Commercial vapor grown carbon nanofibers produced by CVD, Pyrograf®-III PR 24 LHT XT (ASI, Cedarville, OH, USA), were selected to provide electrical properties to the cotton fabrics. This type of carbon nanofibers are synthesized by feeding a mixture of CH_4, NH_3, Air, H_2S, $Fe(CO)_5$ in a horizontal reactor. The carbon nanofibers are abundantly produced in the reactor maintained at 1100 °C when the catalyst nanoparticles from the decomposition of $Fe(CO)_5$ are properly dispersed and activated with the hydrogen sulfide (Tibbetts et al. 2007). The highly disordered outer carbon layer of the as-grown CNFs is partially removed or graphitized by a following thermal post-treatment at 1500 °C in inert atmosphere (Tessonnier et al. 2009; Tibbetts et al. 2007). The PR 24 LHT XT fibers have average diameters of around 100 nm, and present a dual wall structure surrounding the hollow tubular core with a diameter of around 20 nm (Fig. 1a), and lengths ranging from 50 to 100 μm with thermal conductivities around 1000 W/mK (Mahanta et al. 2013). All the other materials used in this work were purchased from Sigma-Aldrich and were used without further purification.

Preparation of samples

Three different type of dip-coated cotton fabrics were produced. Firstly, 5 mg mL^{-1} of sodium dodecylbenzenesulfonate (SDBS) surfactant was dissolved in distilled water. A concentration of 3.2 mg mL^{-1} of CNFs were then added to that surfactant solution. After this, the CNF solution was dispersed through tip

sonication (ultrasonic homogenizer CY-500; 60% power, 5 min) to prepare the CNF ink dispersion. A series of six square pristine fabrics (2×2 cm^2) CWF1, CWF2 and CWF3 were then dipped in the CNF ink solution for 5 min. Then, they were dried in an oven at 80 °C for 10 min. This process was made five times. Before testing, the samples were washed by dipping in distilled water during 10 min, followed by a drying procedure in oven at 80 °C for 10 min. This process was repeated four times. Finally, a new dipping in ethanol for 10 min and drying for 10 min was made to ensure the complete removal of SDBS. The dip-coated fabric samples are named as CWF1@CNF, CWF2@CNF and CWF3@CNF for the remainder of this study.

Morphological and structural analysis

The PR 24 LHT XT fibers were imaged with a JEOL JEM-2100 electron microscope operating a LaB6 electron gun at 80 kV and acquired with an "One-View" 4 k × 4 k CCD camera at minimal under-focus to get that surface layers of the CNFs were visible. Morphological analysis of CWF1, CWF2 and CWF3 and dip-coated samples were carried out in an Ultra-high resolution Field Emission Gun Scanning Electron Microscopy (FEG-SEM), NOVA 200 Nano SEM, FEI Company. Infrared measurements (FTIR) were performed at room temperature with Avatar TM 360 in ATR mode from 4000 to 650 cm^{-1}. FTIR spectra were collected with 32 scans and a resolution of 16 cm^{-1}. FTIR of pristine CNFs was obtained in the reflection standard mode of a CNF pastille and then converted to transmission spectra (using the approximation T = 1 − R). Raman spectroscopy measurements were carried out on an ALPHA300 R Confocal Raman Microscope (WITec) using 532 nm laser for excitation in back scattering geometry. The laser beam with P = 0.5 mW was focused on the sample by a 50× lens (Zeiss), and the spectra was collected with 600 groove/mm grating using 5 acquisitions with 2 s acquisition time. The X-ray photoelectron spectroscopy (XPS) measurements were performed in an ultra-high vacuum (UHV) system ESCALAB250Xi (Thermo Fisher Scientific). The base pressure in the system was below 5×10^{-10} mbar. XPS spectra were acquired with a hemispherical analyzer and a monochromated X-ray source (Al K$_\alpha$ radiation, hv = 1486.6 eV) operated at 15 keV and power 200 W.

The XPS spectra were recorded with pass energies 20 eV, energy step 0.1 eV and 200 eV, energy step 1 eV for high resolution and survey spectra, respectively. The spectrometer was calibrated by setting the Au 4f$_{7/2}$ level to 84.0 eV measured on a gold foil and Ag 2p$_{3/2}$ 932.6 eV on a silver foil. The XPS spectra were peak-fitted using Avantage data processing software. The Shirley-type background subtraction was used for peak fitting, and the quantification was done by using the elemental sensitivity factors provided by the Avantage library.

Thermoelectric analysis

A home built four point probe station was used for electrical conductivity measurements at room temperature and ambient atmosphere. The Agilent 6614 System DC power supply integrated with a Keithley 6485 picoammeter was used for recording current applied, and voltage generated between the two internal probes measured by a Keithley 2000 Multimeter. The thickness of the dip-coated 2×2 cm^2 fabrics was measured by using a precision thickness gauge. Briefly, the sample was kept on a flat anvil and a circular pressure foot was pressed on it from the top under a standard fixed load of 18 Pa. The electrical conductivity was calculated by the equation (Valdes 1954):

$$\sigma = \frac{\ln(2)}{\pi t} \cdot \frac{1}{R} \tag{1}$$

where R is the electric resistance measured, and t is fabric's thickness. Averages values from five measurements on different points within the central area of the three fabric samples were calculated for each fabrication condition. The Seebeck coefficient was measured by the MMR Seebeck Effect Measurement System at 300 K controlled by K20 digital temperature controller, and small temperature difference (1–3 K) was obtained by SB100 digital Seebeck controller with 25 mW power for 30 s. A reference constantan wire sample was used to measure the temperature difference. The 2×2 cm^2 dip-coated fabrics were cut into strips of about 2 mm × 5 mm and connected by silver paint on the test stage. Each specimen was tested 10 times at least, and then the average values of three specimens were calculated. Finally, the figure of merit zT was estimated using a value of thermal conductivity of 0.43 W/(m K), which

Table 1 Constructional parameters and physical properties of the cotton woven fabrics

Fabric parameters	CWF1	CWF2	CWF3
Weave pattern	1/1 plain	1/1 plain	1/1 plain
Linear density (tex)	14.9×20.2	16.3×19.1	16.7×19.7
Warp $\times$ weft yarns (cm^{-1})	35.0×14.0	35.0×23.0	35.0×30.0
Fabric mass $(g\ m^2)$	93.35	104.0	121.1
Fabric thickness at 18 Pa (mm)	0.26	0.26	0.26
Fabric density $(g\ cm^{-3})$	0.36	0.4	0.47
Fabric porosity (%)*	76.7	74.0	69.74

*Porosity (%) = $1 -$ [Fabric density (g/cm^3)/Fibre density (for cotton, $1.54\ g/cm^3$)] $\times 100$
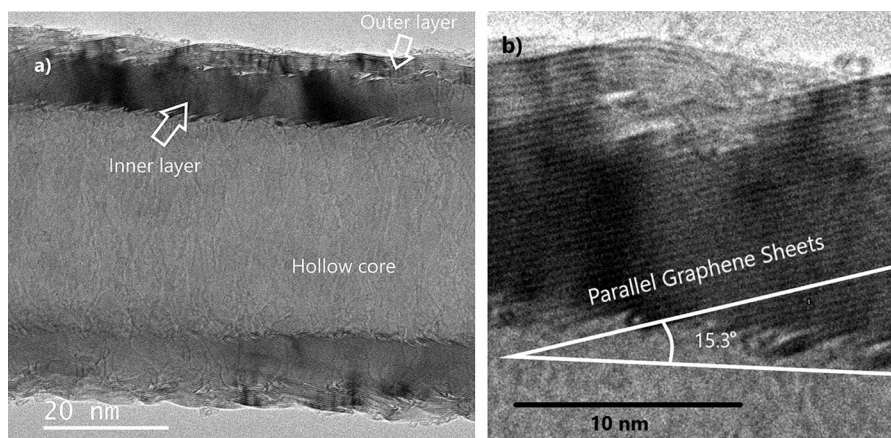
Fig. 1 TEM image of Pyrograf®-III PR 24 LHT XT vapor grown carbon nanofibers (**a**) inner layer constituted of parallel graphene sheets with angles around 15° with respect to the hollow core axis (**b**)

was obtained from a previous investigation based on anisotropic paper-like mats of 0.5 vol% of Pyrograf®-III CNF (Mahanta et al. 2010).

Computer models

The doping effect of the cotton on the electronic properties of CNF graphitic shells was studied by computer modelling with a simplified model. For this, we computed the molecular geometry and the charge transfer of a single linear cellulose nonamer adsorbed onto a finite hexagonal graphene flake with a diameter of 5.6 nm and 912 atoms (Fig. 2) with the GFN1-xTB Hamiltonian. The GFN1-xTB (Geometry, Frequency, Non-covalent, eXtended Tight-Binding) is a recent semiempirical method developed by Grimme et al. (2017) that allows computing efficiently systems with thousands of atoms. The charge transfer was then computed by adding up the CM5 partial charges

(Marenich et al. 2012), which are specially suitable for condensed phases of the cellulose nonamer and the hexagonal graphene flake.

Results

Morphological and structural analysis

A representative TEM image of Pyrograf®-III PR 24 LHT XT is shown in Fig. 1. This particular grade shows a dual wall structure (Fig. 1a). The inner layer with a diameter of around 10 nm shows parallel graphene sheets with angles around 15° with respect to the hollow core axis (Fig. 1b). On the other hand, the thermal post-treatment at 1500 °C for this particular grade, causes the graphene sheets of the narrower outer layer to align parallelly to the main axis. Moreover, some voids are formed between both layers

as it was also observed in TEM analysis of a different grade of Pyrograf®-III CNFs with higher thermal post-treatments of 3000 °C (Tessonnier et al. 2009). Scanning electron microscopy images of pristine and dip-coated cotton woven fabrics are shown in Fig. 3. The constructional parameters and physical properties of the pristine cotton woven fabrics are described in Table 1. The main difference between the three pristine cotton fabrics (Fig. 3a–c) is the void size formed between warp and weft yarns. These voids are clearly higher in CWF1 samples (Fig. 3a) with square dimensions of around 250×250 μm^2, whereas CWF2 (Fig. 3b) and CWF3 (Fig. 3c) samples show smaller sizes of around 170×170 and 100×100 μm^2, respectively. The square voids observed in pristine cotton woven fabrics clearly change the surface morphology of the dip-coated fabrics. The original cotton fabric structure of CWF1 and CWF2 is clearly noticed on the surface of CWF1@CNF (Fig. 3d), and in a less extent in dip-coated samples CWF2@CNF (Fig. 3e). On the contrary, the layer of carbon nanofibers in sample CWF3@CNF (Fig. 3f) totally hides the voids of the original cotton fabric CWF3. This different morphology observed in sample CWF3@CNF can be explained by the void´s size of CWF3, close to the maximum length of the CNFs (100 μm), which can cause that all the agglomerates larger than 100 μm remains on the surface. Accordingly, the possibility of peeling off increases in sample CWF3@CNF, as it can be observed in its cross section SEM image (Fig. 3i). We have also calculated the amount of CNFs in dip-coated samples from the difference in weight between the neat and the dip-coated fabrics. Samples CWF1@CNF have shown amounts of 1.13 ± 0.27 mg cm^{-2}, whereas CWF2@CNF and CWF3@CNF showed lower loads of 0.23 ± 0.16 and 0.31 ± 0.07 mg cm^{-2}, respectively. This means that samples CWF1@CNF with the larger voids allow that CNFs can penetrate better under the surface of the cotton fabric, and as result they can retain a higher amount of CNFs than the other two samples CWF2@CNF and CWF3@CNF, whose smaller voids cause that the agglomerates remain on the surface. This worsens the bonding between CNFs and cotton fabric, and it can explain the lower amount of CNFs observed. In conclusion, the different structure of neat cotton woven fabrics used affects ostensibly the surface morphology of dip-coated fabrics despite

samples CWF1@CNF, CWF2@CNF and CWF3@CNF were produced exactly with the same methodology and CNF ink dispersions.

The FTIR spectra of CNFs, uncoated samples CWF1 (CWF2 and CWF3 samples were not plotted because were identical to CWF1), and dip-coated samples CWF1@CNF, CWF2@CNF and CWF3@CNF are shown in Fig. 4. CNFs did not show significant structural information because of their very high absorbance (Arshad et al. 2011), though bands 1550 cm^{-1} and 1210 cm^{-1} corresponding to C=C (Ma et al. 2003) were detected. The spectrum of CWF1 shows the representative features of cellulose. There is a broad band attributed to O–H stretching vibration at 3266 cm^{-1} as well as a peak assigned to C–H stretching vibration at 2896 cm^{-1}. The strong absorption bands at 1156, 1103 and 1023 cm^{-1} come from the overlapping bands assigned to the different chemical groups of cellulose, such as the C–O, C–C and C–O–C stretching vibrations. Finally, the spectra of the dip-coated samples CWF1@CNF, CWF2@CNF and CWF3@CNF confirm that the peaks previously described and assigned to cellulose disappear after the addition of CNFs with the sole exception of the absorption band at 1023 cm^{-1}. It is possible to observe a decrease in transmittance in the region from 4000 to 3000 cm^{-1} in the dip-coated samples, which is more pronounced for samples CWF1@CNF and CWF3@CNF, thus indicating the contribution from the CNFs. Therefore, it is clear that the FTIR spectra of the cotton fabric changes after the CNF addition. Indeed, the absence of the characteristics peaks of the cellulose in the coated samples, it has been also observed by Fig. 5, which shows the Raman spectra of CNFs, uncoated samples CWF1 (neat samples CWF2 and CWF3 were not plotted because they show the same Raman spectra as CWF1), and dip-coated samples. The spectra of CNFs presents the characteristic three Raman bands found in similar carbon materials. The disorder-induced phonon mode D band around 1350 cm^{-1}, related to disordered structures in carbon materials (Lehman et al. 2011). The G-band, around 1580 cm^{-1}, corresponding to the degenerate in-plane E_{2g} optical mode at the center of the Brillouin zone, characteristic of the graphitic lattice vibration mode, and generally used to identify well-ordered CNTs (Wang et al. 1990), and the 2D band at ≈ 2700 cm^{-1} (also called G′ band), which corresponds to a second-order Raman process

Fig. 2 Optimized molecular geometries of basal (**a**) and on-edge cellulose nonamer (**b**) adsorption on a $C_{834}H_{78}$ hexagonal graphene flake computed with a xTB-GFN1 Hamiltonian
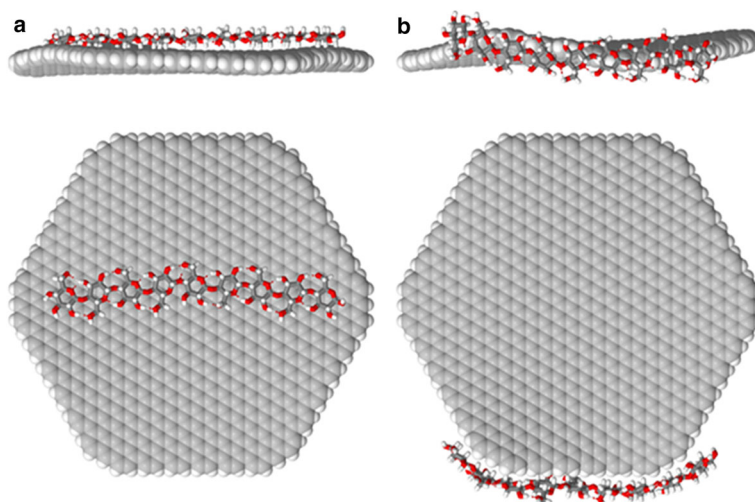

involving two phonons close to the zone boundary K point (Endo et al. 2001). On the other hand, the CWF1 presents the signatures of cellulose in four main ranges (Nakanishi et al. 1999): the range 250–550 cm^{-1}, related with bending modes involving COC, OCC and OCO vibrations, the range 800–1200 cm^{-1}, related with HCC, HCO bendings, COC stretching symmetry and CO, CC stretching symmetry (Szymańska-Chargot et al. 2011), the range 1200–1500 cm^{-1}, related with HCH, HCC, HOC wagging, rocking, twisting and scissoring, and 3000 cm^{-1} corresponding to CH stretching vibrations (Szymańska-Chargot et al. 2011).

Finally, the dip-coated samples present the same signature of the CNFs. The peak position, the full width half maximum (FWHM) of the D and G modes and the intensity ratio between D and G modes (I_D/I_G) were calculated by fitting the Raman spectra with Lorentzian functions, and the results are presented in Table 2. We have only analyzed the D and G bands since the 2D band shows low intensity. A shift to lower wavenumbers of the G and D peak positions between the CNFs and dip-coated samples together with a FWHM decrease is observed. Furthermore, the intensity ratios I_D/I_G, typically used to characterize the degree of order in carbon materials (Liu et al. 2004), decreases slightly in dip-coated samples. This is an indication of a higher regularity in the carbon network induced by the structure of the neat cotton fabrics and the dip-coating methodology used.

The chemical composition of CNFs, pristine CWF1, and dip-coated samples was also analyzed by

XPS. All samples contain mainly carbon and oxygen, as it is evidenced by the survey XPS spectra (Fig. 6), though some traces of sulphur ($\sim$ 0.1 at%) were also detected in CNFs and dip-coated samples. The C/O concentration ratios were calculated from the peaks C1s and O1s, and presented in Table 3. The composition analysis of pristine CNFs revealed a small amount of oxygen ($\sim$ 1.76 at%), which can be assigned to C–O and C=O functional groups. A comparison of the deconvolution of C1s and O1s spectra for neat CNF and sample CWF3@CNF is presented in Fig. 7. The C1s spectra showed a strong line at binding energy (BE) of $\sim$ 284.4 eV, which together with the "satellite" peaks represent sp^2 hybridized carbon (Fig. 7a–c). An additional contribution from C–O and C=O oxygen functional groups were also observed for CNFs and CWF3@CNF samples. The O1s spectra in CNFs (Fig. 7b) yielded peaks at $\sim$ 531.9 and $\sim$ 533.5 eV assigned to C–O and C=O, respectively, whereas CWF1@CNF, CWF2@CNF and CWF3@CNF samples yielded a wide asymmetric peak at $\sim$ 532.5 eV (Fig. 7d). Noteworthy, the O1s and C1s XPS survey spectra from the CWF2@CNF and CWF3@CNF samples are quite similar in shape (Fig. 6) and they show also similar C/O concentration ratios, while the spectra taken from sample CWF1@CNF are dominated by signals belonging to the starting cotton fabric. It can be assumed that the stronger contribution from the cotton points out to lower surface density of the CNF coating in samples CWF1@CNF. We assume therefore that the higher dimensions of the voids in CWF1 (Fig. 3)
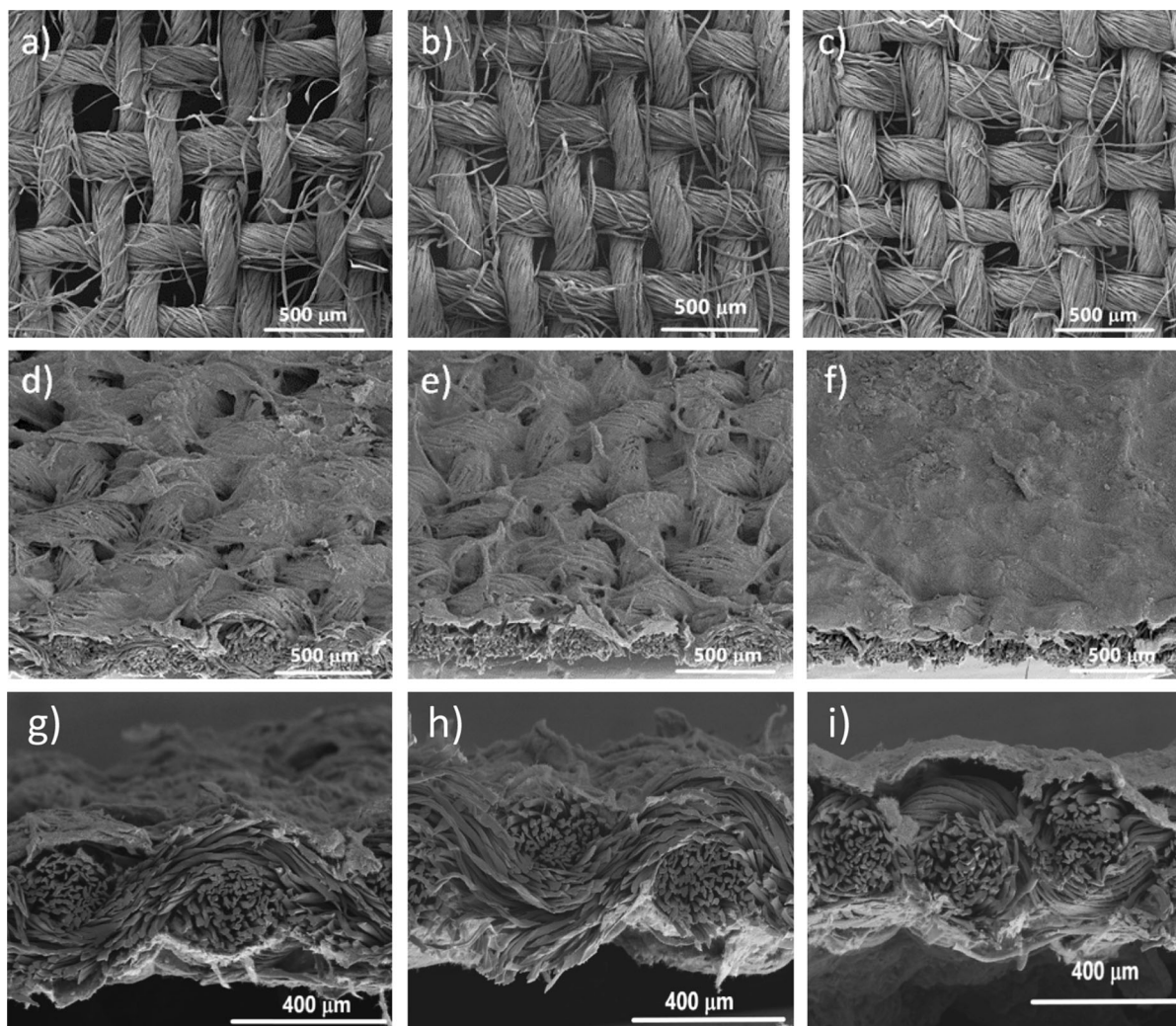
Fig. 3 SEM images of uncoated cotton fabrics: CWF1 (**a**), CWF2 (**b**) and CWF3 (**c**); surfaces of dip-coated cotton fabrics: CWF1@CNF (**d**), CWF2@CNF (**e**) and CWF3@CNF (**f**); and cross sections of dip-coated cotton fabrics: CWF1@CNF (**g**), CWF2@CNF (**h**) and CWF3@CNF (**i**)

clearly facilitate a higher penetration of CNFs into the whole fabric than in the cases of samples CWF2@CNF and CWF3@CNF, where most of CNFs remain on the surface of the cotton fabric.

Thermoelectric analysis

The electrical conductivities at room temperature of the dip-coated CNF-based cotton fabrics are represented in Fig. 8 (triangular symbols). The results show that σ varies as a function of the interstitial void size of the neat cotton fabrics used. The samples CWF1@CNF produced from the cotton woven fabric with the largest voids between yarns (250×250 μm^2) showed the lowest σ of 21.6 ± 3.6 S m^{-1}, whereas samples CWF3@CNF with the smallest voids (100×100 μm^2) showed the highest σ values of 27.3 ± 2.0 S m^{-1}. This variation of the conductivity in CWF1@CNF and samples CWF3@CNF can be explained by the differences in the morphology of their surfaces observed in Fig. 3d–f. Despite the lower amount of CNFs trapped in samples CWF3@CNF, the smaller voids in CWF3 seem to promote networks with agglomerates closer to each other and higher number of conductive pathways than in CWF1@CNF, which can explain the slightly
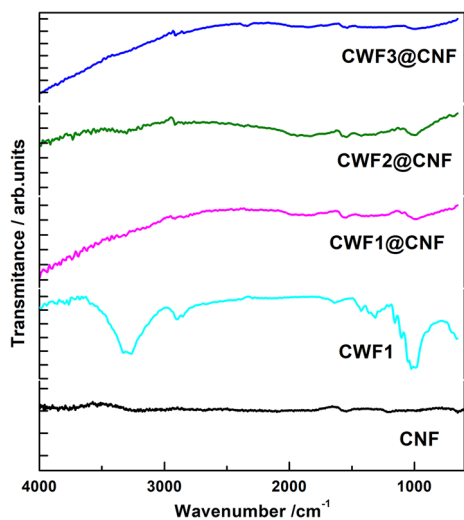
Fig. 4 FTIR spectra of pristine CNFs, uncoated sample CWF1 and dip-coated samples CWF1@CNF, CWF2@CNF and CWF3@CNF
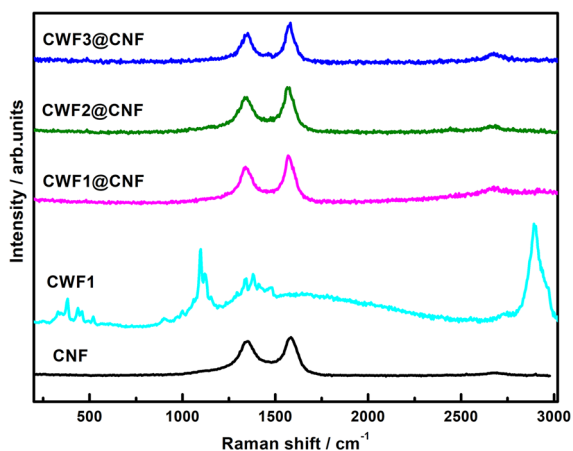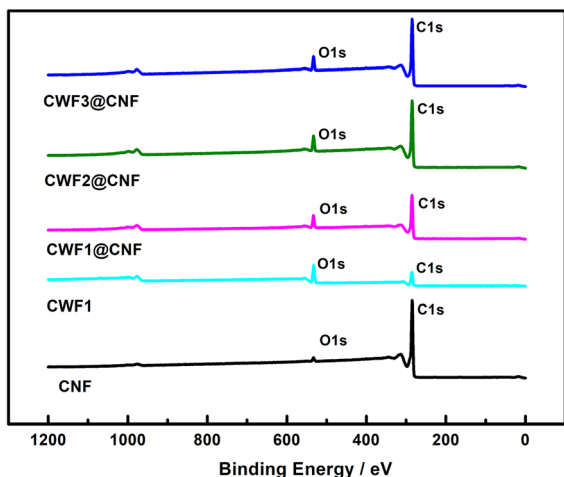

Fig. 5 Raman spectra of pristine CNFs, uncoated sample CWF1 and dip-coated samples CWF1@CNF, CWF2@CNF and CWF3@CNF

higher conductivity found in samples CWF3@CNF. Moreover, we cannot exclude the possibility of a slight e^- charge transfer or n-doping from the cellulose onto the most external CNF graphitic shells in all dip-coated samples, as we shall discuss below. Our values (~ 0.3 S cm^{-1}) are in the range of the as-prepared PEDOT:PSS coated polyester fabrics (~ 0.5 S cm^{-1}) (Du et al. 2015), but they are lower than the σ of 1 S cm^{-1} reported for PET sewing threads coated with MWCNTs and PVP (Ryan et al. 2018). They are also lower than the values of 5 S cm^{-1} reported in the

pioneering work of Yi Cui et al. based on SWCNT dip-coated cotton fabrics soaked in 4 M nitric acid (Hu et al. 2010). A value of 6 S cm^{-1} has been recently obtained with Pyrograf®-III PR 25 HHT XT CNF based inks sprayed onto cotton fabrics (Cataldi et al. 2019). However, these inks were composed of 40% wt of CNFs (considerably higher than the approximately 5.5 wt% used in our study) and a concentration of 15 mg mL^{-1} of aleuritic acid dispersed in equal volumes of water and ethanol. The thermoelectric power of our samples at room temperature is presented in Fig. 8 (squared symbols). A similar α of -7.6 ± 1.1 µV K^{-1} and -7.9 ± 0.8 µV K^{-1} is observed for samples CWF1@CNF and CWF2@CNF, respectively. These values are similar to our previous TE study of polymer composites based on the same Pyrograf®-III PR 24 LHT XT melt compounded with PP, for which we reported Seebeck coefficients of about -8.5 µV K^{-1} for PP/CNF composites films with up to 5 wt% concentration of CNFs (Paleo et al. 2019). Therefore, it is plausible that this negative Seebeck coefficient is fundamentally caused by the n-type TE character of the CNFs (Pyrograf®-III, PR 24 LHT XT) due to the electrical insulating nature of the cotton woven fabric used in this study, and the PP used in our preceding work. In this respect, we found a previous work reporting negative TEP of around -5.0 µV K^{-1} at room temperature in films of cyanate ester resin (CER) and Pyrograf®-I vapor grown carbon fibers (VGCFs) with high degree of graphitization in their outer layers thanks to their post heat treatment at 2400 °C (Stokes et al. 1996). There, it is explained that this negative TEP is because the VGCFs can be considered as a nearly compensated semimetal, and their transport properties explained by the two-band electronic model, so the partial TEP originating from the two bands oppose each other, resulting in a small and negative TEP. Similarly, the CNFs used in our study may have an analogous compensated semimetal nature, which would explain the small and negative TEP obtained in our dip-coated cotton fabrics. In addition, this particular type of CNFs has a CVD external layer that can covering up the necessary graphitic end planes to graft oxygen functional groups onto them, which it is demonstrated by the very few amount of oxygen observed by XPS in CNFs (1.76%). Therefore, this small amount of oxygen observed could also explain the lack of the inherent doping with

Table 2 Parameters obtained from the Raman fitting

Sample	ω_G (cm^{-1})	FWHM$_G$ (cm^{-1})	ω_D (cm^{-1})	FWHM$_D$ (cm^{-1})	I_D/I_G	L_a (nm)
CNF	1582	90	1349	113	0.91	4.84
CWF1@CNF	1575	70	1345	90	0.77	5.7
CWF2@CNF	1574	67	1343	100	0.80	5.5
CWF3@CNF	1575	65	1346	90	0.80	5.5

Fig. 6 XPS survey spectra: pristine CNFs, uncoated sample CWF1 and dip-coated samples CWF1@CNF, CWF2@CNF and CWF3@CNF

oxygen found in most of CNTs and the n-type character of the CNFs used in our work. Furthermore, the higher graphitization of the two outer layers caused by the thermal post-treatment at 1500 °C, as evidenced by the TEM imaging (Fig. 1a), could explain the slightly higher TEP (absolute value) from − 5 (Stokes et al. 1996) to − 8 µV K^{-1} observed in our samples CWF1@CNF and CWF2@CNF. On the other hand, the samples CWF3@CNF with the highest conductivity, showed the lowest TEP of − 5.0 µV K^{-1} ± 1.1 µV K^{-1}. This decrease in TEP matches with the behavior of heterogeneous conducting polymer composites, where a decreasing of TEP as function of the higher conductivity is attributed to the inverse σ dependence of the energy barrier term in the thermal fluctuation induced tunneling model (Hewitt et al. 2011; Luo et al. 2016). We have also studied the effect of the cellulose fibers from cotton on the most external shells of the CNFs by computer models as it is described in "Computer models" section, where the CNF outer wall is represented by a graphene nanoflake, and two different adsorptions geometries are studied: basal (representing a graphitized CNF, Fig. 2a) and on-edge (representing a non-graphitized CNF, Fig. 2b). These two adsorption modes are radically different and consequently their binding energy differs substantially: the basal adsorption is strongly favoured, 4.4 eV, while the on-edge adsorption shows a considerably reduced value, 1.13 eV. The charge transfer also differs strongly from 0.47 e^{-} (basal) to 0.10 e^{-} (on-edge) which correspond to 0.05 e^{-} and 0.01 e^{-} per cellulose monomer respectively. In addition, the effect of different local environments was evaluated by comparatively computing the molecular geometry and charge transfer in vacuum and in a continuum of water yielding quite similar results. The adsorption of cellulose parallel to graphene (basal)

Table 3 Summary of the C1s and O1s content for carbon sp2, adventitious carbon, π–π* satellite, C–O, and C=O species

Sample	C/O	Carbon (%)					Oxygen (%)		
		C sp2	adventitious carbon	C–O, C=O	π–π* satellite	C–O/C = O	O–C	O=C	O$_{Total}$
CNF	50	84.5	–	4.7	8.9	0.53	0.9	0.9	1.8
CWF1	2.3	38.4	28.7	8.2	–	4.38	–	–	32.3
CWF1&CNF	8.6	49.8	12.2	22.9	5.1	4.49	–	–	9.9
CWF2&CNF	10.3	59.1	8.9	18.3	5.1	3.59	–	–	8.4
CWF3&CNF	10.9	58.3	8.1	20.8	4.8	4.33	–	–	8.0

Total concentration ratios C/O are also showed
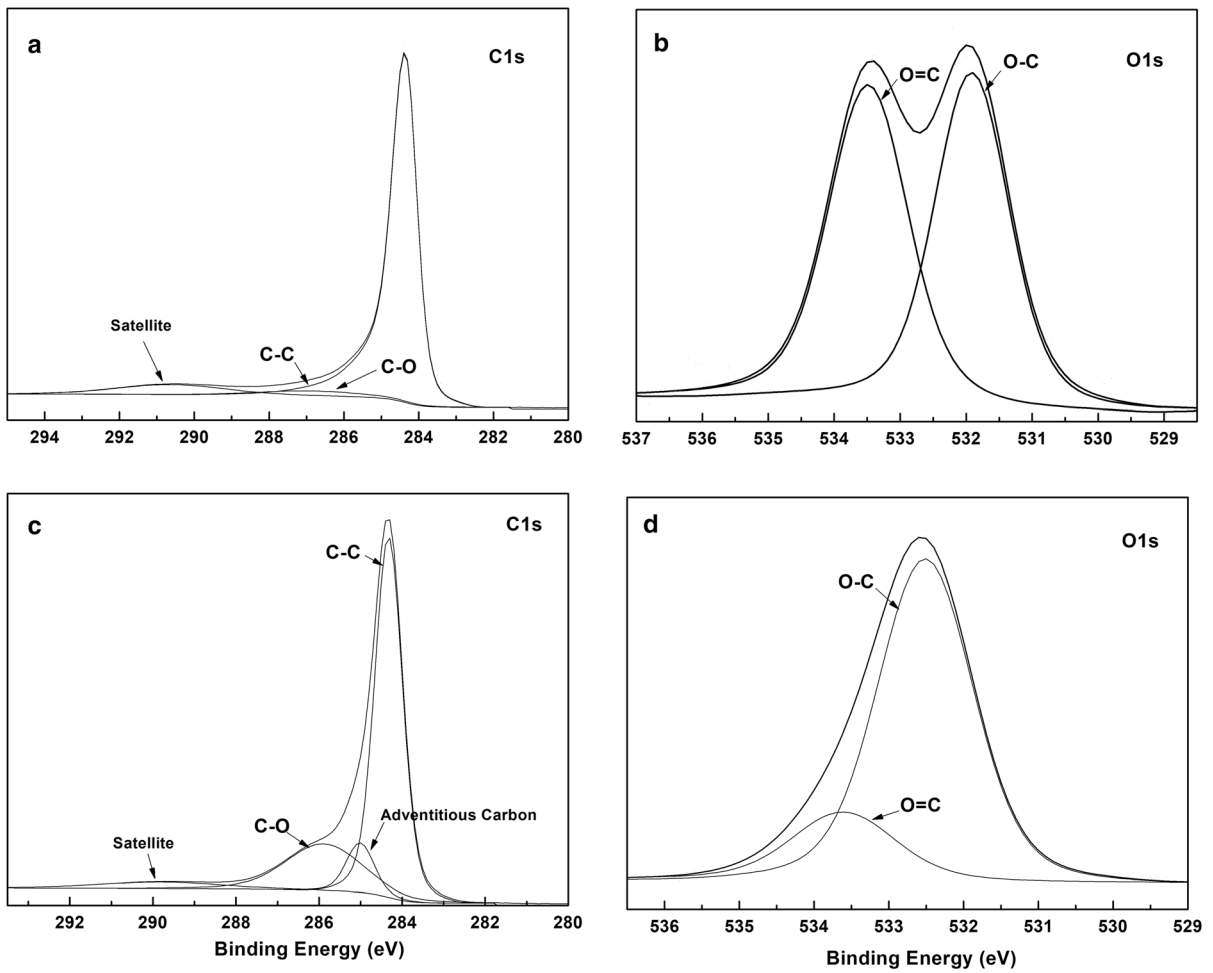
Fig. 7 XPS deconvolution: C1s (**a**) and O1s (**b**) of pristine CNFs; C1s (**c**) and O1s (**d**) of dip-coated sample CWF3@CNF
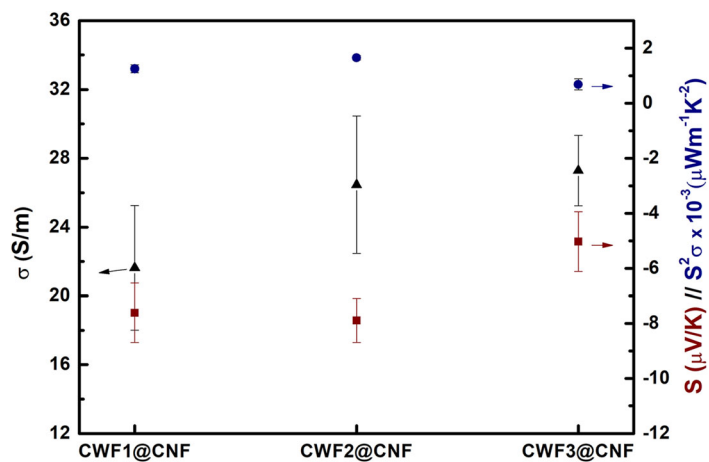

Fig. 8 Electrical conductivity (triangular points), negative Seebeck coefficient (squared points), and Power factor $\times\ 10^{-3}$ (circular points) of dip-coated cotton fabrics

yields an n-doped material by 0.47 e⁻ in vacuum and 0.44 e⁻ in water. These results indicate that cellulose (and thus cotton) should induce some n-doping on available graphitic planes of the CNFs where basal adsorption is possible. It must be noted that, to the best of our knowledge, this is the first report of n-type TE textiles directly obtained by using carbon nanostructures (including CNT, and other 2D carbon nanostructures such as graphene and their derivatives) without the need for additional physical or chemical doping methods during processing (Lan et al. 2019; Ryan et al. 2018). Surprisingly, the n-type TE character of our samples is in contrast with the already mentioned work (Cataldi et al. 2019), where Pyrograf®-III PR 25 HHT XT CNF based inks sprayed onto cotton fabrics showed positive TEP of 6.4 ± 0.5 μV K⁻¹. The type of Pyrograf®-III CNF used in that work has a considerably higher heat-treatment (3000 °C) than the Pyrograf®-III CNF used in our study (1500 °C) (Tessonnier et al. 2009), and consequently, they should have a higher grade of graphitization of their outer layers, which should also cause an intrinsic negative TEP of the CNFs. Yet, the presence of other species, like the aleuritic acid, or the cellulose itself may alter the doping degree of CNFs, as we discuss in this study. In comparative terms, our α is far from the TEP of -58 μV K⁻¹ at room temperature already reported in cotton yarns soaked with SWCNTs, though in that study, the authors add 5 wt% of polyethyleneimine (PEI) solution during processing to get their negative TEP (Lan et al. 2019). Finally, the power factor at room temperature was also calculated and the results are shown in Fig. 8 (squared symbols). The PF varies slightly depending on the three different textile substrates with values of 1.25×10^{-3} μW m⁻¹ K⁻² and 1.65×10^{-3} μW m⁻¹ K⁻² for samples CWF1@CNF and CWF2@CNF, respectively, whereas the samples CWF3@CNF showed the lowest PF (0.69×10^{-3} μW m⁻¹ K⁻²). PF of 4.1×10^{-3} μW m⁻¹ K⁻² was reported in standard cotton dip-dyed with PEDOT:PSS (Guo et al. 2016). Our results are one order of magnitude lower than 2.5×10^{-2} μW m⁻¹ K⁻² reported in cotton fabrics sprayed with ink of aleuritic acid and Pyrograf®-III PR 25 HHT XT CNFs (Cataldi et al. 2019). PF of 7.4×10^{-1} μW m⁻¹ K⁻² were also reported for cotton yarns soaked with a commercial p-type SWCNT (Lan et al. 2019). The highest zT of 1.14×10^{-6} at room temperature for samples CWF2@CNF was also calculated from the experimental values of σ and α obtained in this study, and the estimated thermal conductivity value of 0.43 W/(m K) reported for buckypapers of 0.5 vol% of Pyrograf®-III PR 25 carbon nanofibers (Mahanta et al. 2010). Our best values are in the same order of magnitude than the work based on polyester coated with SWCNTs and PANI (Li et al. 2016), which presents a zT of 6×10^{-6}. Though, they are one order lower than the work which uses inks based on Pyrograf®-III PR 25 HHT XT CNFs onto cotton fabrics 1.7×10^{-5} (Cataldi et al. 2019), when considering the same estimation of 0.43 W/(m K) for the thermal conductivity.

Conclusions

Commercial vapor grown carbon nanofibers with hollow tubular cores surrounded by two highly graphitized outer layers were used for producing CNF-based ink dispersions and dip-coating three woven cotton fabrics with different constructional parameters. The morphologic, structural and thermoelectric properties of the dip-coated CNF cotton fabrics were analyzed. Unlike the positive thermoelectric power generally observed in thermoelectric textile fabrics produced with similar carbon-based nanostructures such as carbon nanotubes, all the dip-coated cotton fabrics showed small negative TEP. This n-type character can be explained by the compensated semimetal character of CNFs and the high graphitization of the CNF outer layers that can covering up the necessary graphitic end planes to graft oxygen functional groups onto them. The morphological analysis showed that the surface was changed markedly as function of the woven cotton fabric structure. The best dip-coated cotton fabrics showed negative TEP values around -8 μV K⁻¹ and a maximum power factor of 1.65×10^{-3} μW m⁻¹ K⁻², corresponding to a figure of merit of 1.14×10^{-6} at room temperature. Moreover, a slight doping effect of the cotton on the electronic properties of the most external CNF graphitic shells was also detected by computer modelling. In conclusion, this work demonstrated that n-type thermoelectric carbon-based textile fabrics can be produced easily without the functionalization processes and/or additives normally found in the state-of-art to avoid the inherent doping with oxygen,

which causes the typical p-type character found in most carbon-based TE materials.

Compliance with ethical standards

Conflict of interest The authors declare that they have no conflict of interest.

References

Arshad SN, Naraghi M, Chasiotis I (2011) Strong carbon nanofibers from electrospun polyacrylonitrile. Carbon 49:1710–1719. https://doi.org/10.1016/j.carbon.2010.12.056

Beretta D et al (2019) Thermoelectrics: from history, a window to the future. Mater Sci Eng R Rep. https://doi.org/10.1016/j.mser.2018.09.001

Blackburn JL, Ferguson AJ, Cho C, Grunlan JC (2018) Carbon-nanotube-based thermoelectric materials and devices. Adv Mater. https://doi.org/10.1002/adma.201704386

Cataldi P, Cassinelli M, Heredia-Guerrero JA, Guzman-Puyol S, Naderizadeh S, Athanassiou A, Caironi M (2019) Green biocomposites for thermoelectric wearable applications. Adv Funct Mater. https://doi.org/10.1002/adfm.201907301

Du Y, Cai K, Chen S, Wang H, Shen SZ, Donelson R, Lin T (2015) Thermoelectric fabrics: toward power generating clothing. Sci Rep-UK. https://doi.org/10.1038/srep06411

Endo M, Tamagawa I, Koyama T (1977) Thermoelectric power of carbon fibers prepared from benzene. Jpn J Appl Phys 16:1771–1774. https://doi.org/10.1143/JJAP.16.1771

Endo M, Kim YA, Takeda T, Hong SH, Matusita T, Hayashi T, Dresselhaus MS (2001) Structural characterization of carbon nanofibers obtained by hydrocarbon pyrolysis. Carbon 39:2003–2010. https://doi.org/10.1016/S0008-6223(01)00019-7

Francioso L, De Pascali C, Taurino A, Siciliano P, De Risi (2013) A Wearable and flexible thermoelectric generator with enhanced package. In: Proc SPIE Int Soc Opt Eng. https://doi.org/10.1117/12.2017385

Grimme S, Bannwarth C, Shushkov P (2017) A robust and accurate tight-binding quantum chemical method for structures, vibrational frequencies, and noncovalent interactions of large molecular systems parametrized for all spd-block elements (Z = 1-86). J Chem Theory Comput 13:1989–2009. https://doi.org/10.1021/acs.jctc.7b00118

Guo Y, Otley MT, Li M, Zhang X, Sinha SK, Treich GM, Sotzing GA (2016) PEDOT:PSS "wires" printed on textile for wearable electronics. ACS Appl Mater Interfaces 8:26998–27005. https://doi.org/10.1021/acsami.6b08036

Heremans J, Beetz CP Jr (1985) Thermal conductivity and thermopower of vapor-grown graphite fibers. Phys Rev B 32:1981–1986. https://doi.org/10.1103/PhysRevB.32.1981

Hewitt CA, Kaiser AB, Roth S, Craps M, Czerw R, Carroll DL (2011) Varying the concentration of single walled carbon nanotubes in thin film polymer composites, and its effect on thermoelectric power. Appl Phys Lett. https://doi.org/10.1063/1.3580761

Hu L et al (2010) Stretchable, porous, and conductive energy textiles. Nano Lett 10:708–714. https://doi.org/10.1021/nl903949m

Ito M, Koizumi T, Kojima H, Saito T, Nakamura M (2017) From materials to device design of a thermoelectric fabric for wearable energy harvesters. J Mater Chem A 5:12068–12072. https://doi.org/10.1039/c7ta00304h

Kang D, Park N, Ko JH, Bae E, Park W (2005) Oxygen-induced p-type doping of a long individual single-walled carbon nanotube. Nanotechnology 16:1048–1052. https://doi.org/10.1088/0957-4484/16/8/008

Karttunen AJ, Sarnes L, Townsend R, Mikkonen J, Karppinen M (2017) Flexible thermoelectric ZnO–organic superlattices on cotton textile substrates by ALD/MLD. Adv Electron Mater. https://doi.org/10.1002/aelm.201600459

Kim JY, Mo JH, Kang YH, Cho SY, Jang KS (2018) Thermoelectric fibers from well-dispersed carbon nanotube/poly(vinyliedene fluoride) pastes for fiber-based thermoelectric generators. Nanoscale 10:19766–19773. https://doi.org/10.1039/c8nr06415f

Lan X et al (2019) A high performance all-organic thermoelectric fiber generator towards promising wearable electron. Compos Sci Technol. https://doi.org/10.1016/j.compscitech.2019.107767

Lehman JH, Terrones M, Mansfield E, Hurst KE, Meunier V (2011) Evaluating the characteristics of multiwall carbon nanotubes. Carbon 49:2581–2602. https://doi.org/10.1016/j.carbon.2011.03.028

Li P, Guo Y, Mu J, Wang H, Zhang Q, Li Y (2016) Single-walled carbon nanotubes/polyaniline-coated polyester thermoelectric textile with good interface stability prepared by ultrasonic induction. RSC Adv 6:90347–90353. https://doi.org/10.1039/c6ra16532j

Li C, Jiang F, Liu C, Liu P, Xu J (2019) Present and future thermoelectric materials toward wearable energy harvesting. Appl Mater Today 15:543–557. https://doi.org/10.1016/j.apmt.2019.04.007

Liu Y, Pan C, Wang J (2004) Raman spectra of carbon nanotubes and nanofibers prepared by ethanol flames. J Mater Sci 39:1091–1094. https://doi.org/10.1023/B:JMSC.0000012952.20840.09

Luo J, Krause B, Pötschke P (2016) Melt-mixed thermoplastic composites containing carbon nanotubes for thermoelectric applications. AIMS Mater Sci 3:1107–1116. https://doi.org/10.3934/matersci.2016.3.1107

Ma H, Zeng J, Realff ML, Kumar S, Schiraldi DA (2003) Processing, structure, and properties of fibers from

polyester/carbon nanofiber composites. Compos Sci and Technol 63:1617–1628. https://doi.org/10.1016/s0266-3538(03)00071-x

Mahanta NK, Abramson AR, Lake ML, Burton DJ, Chang JC, Mayer HK, Ravine JL (2010) Thermal conductivity of carbon nanofiber mats. Carbon 48:4457–4465. https://doi.org/10.1016/j.carbon.2010.08.005

Mahanta NK, Abramson AR, Howe JY (2013) Thermal conductivity measurements on individual vapor-grown carbon nanofibers and graphene nanoplatelets. J Appl Phys. https://doi.org/10.1063/1.4827378

Marenich AV, Jerome SV, Cramer CJ, Truhlar DG (2012) Charge model 5: an extension of hirshfeld population analysis for the accurate description of molecular interactions in gaseous and condensed phases. Chem Theory Comput 8:527–541. https://doi.org/10.1021/ct200866d

McGrail BT, Sehirlioglu A, Pentzer E (2015) Polymer composites for thermoelectric applications. Angew Chem Int Edit 54:1710–1723. https://doi.org/10.1002/anie.201408431

Miao J, Miyauchi M, Simmons TJ, Dordick JS, Linhardt RJ (2010) Electrospinning of nanomaterials and applications in electronic components and devices. J Nanosci Nanotechnol 10:5507–5519. https://doi.org/10.1166/jnn.2010.3073

Minus M, Kumar S (2005) The processing, properties, and structure of carbon fibers. JOM 57:52–58. https://doi.org/10.1007/s11837-005-0217-8

Nakanishi K, BMP, Meth-Cohn O, Barton DHR (1999). In: Comprehensive natural products chemistry: carbohydrates and their derivatives including tannins, cellulose and related lignins, vol 3. Pergamon Pr, pp 529–598

Paleo AJ et al (2019) Negative thermoelectric power of melt mixed vapor grown carbon nanofiber polypropylene composites. Carbon 150:408–416. https://doi.org/10.1016/j.carbon.2019.05.035

Rowe DM (1995) CRC handbook of thermoelectrics. CRC press

Ryan JD, Mengistie DA, Gabrielsson R, Lund A, Müller C (2017) Machine-washable PEDOT:PSS dyed silk yarns for electronic textiles. ACS Appl Mater Interfaces 9:9045–9050. https://doi.org/10.1021/acsami.7b00530

Ryan JD, Lund A, Hofmann AI, Kroon R, Sarabia-Riquelme R, Weisenberger MC, Müller C (2018) All-organic textile thermoelectrics with carbon-nanotube-coated n-type yarns. ACS Appl Energy Mater 1:2934–2941. https://doi.org/10.1021/acsaem.8b00617

Snyder GJ, Toberer ES (2008) Complex thermoelectric materials. Nat Mater 7:105–114. https://doi.org/10.1038/nmat2090

Stokes KL, Tritt TM, Fuller-Mora WW, Ehrlich AC, Jacobsen RL (1996) Electronic transport properties of highly conducting vapor-grown carbon fiber composites. In: International conference on thermoelectrics, ICT, proceedings, pp 164–167

Szymańska-Chargot M, Cybulska J, Zdunek A (2011) Sensing the structural differences in cellulose from apple and bacterial cell wall materials by Raman and FT-IR Spectroscopy. Sensors 11:5543–5560. https://doi.org/10.3390/s110605543

Tessonnier JP et al (2009) Analysis of the structure and chemical properties of some commercial carbon nanostructures. Carbon 47:1779–1798. https://doi.org/10.1016/j.carbon.2009.02.032

Tibbetts GG, Lake ML, Strong KL, Rice BP (2007) A review of the fabrication and properties of vapor-grown carbon nanofiber/polymer composites. Compos Sci Technol 67:1709–1718. https://doi.org/10.1016/j.compscitech.2006.06.015

Valdes LB (1954) Resistivity measurements on germanium for transistors. Proc IRE 42:420–427. https://doi.org/10.1109/JRPROC.1954.274680

Veluswamy P, Sathiyamoorthy S, Gomathi PT, Jayabal K, Kumar R, Kuznetsov D, Ikeda H (2019) A novel investigation on ZnO nanostructures on carbon fabric for harvesting thermopower on textile. Appl Surf Sci. https://doi.org/10.1016/j.apsusc.2019.143658

Wang Y, Alsmeyer DC, McCreery RL (1990) Raman Spectroscopy of carbon materials: structural basis of observed spectra. Chem Mater 2:557–563. https://doi.org/10.1021/cm00011a018

Wang L et al (2019) Fabrication of core-shell structured poly(3,4-ethylenedioxythiophene)/carbon nanotube hybrid with enhanced thermoelectric power factors. Carbon 148:290–296. https://doi.org/10.1016/j.carbon.2019.03.088

Wu Q, Hu J (2016) Waterborne polyurethane based thermoelectric composites and their application potential in wearable thermoelectric textiles. Compos B Eng 107:59–66. https://doi.org/10.1016/j.compositesb.2016.09.068

Yee SK, Coates NE, Majumdar A, Urban JJ, Segalman RA (2013) Thermoelectric power factor optimization in PEDOT:PSS tellurium nanowire hybrid composites. Phys Chem Chem Phys 15:4024–4032. https://doi.org/10.1039/c3cp44558e

Yu C, Shi L, Yao Z, Li D, Majumdar A (2005) Thermal conductance and thermopower of an individual single-wall carbon nanotube. Nano Lett 5:1842–1846. https://doi.org/10.1021/nl051044e

Zettl A (2000) Extreme oxygen sensitivity of electronic properties of carbon nanotubes. Science 287:1801–1804. https://doi.org/10.1126/science.287.5459.1801